

## Pyrolysis behaviour and combustion kinetics of waste printed circuit boards

Kang Yan<sup>1,2,4</sup>, Chongwei Liu<sup>1</sup>, Liping Liu<sup>1</sup>, Min Xiong<sup>1</sup>, Jiongtong Chen<sup>1</sup>, Zhongtang Zhang<sup>1,2</sup>,  
Shuiping Zhong<sup>1</sup>, Zhifeng Xu<sup>3,4</sup>,, and Jindi Huang<sup>1</sup>,

1) School of Metallurgy Engineering, Jiangxi University of Science and Technology, Ganzhou 341000, China

2) Ganzhou Engineering Technology Research Center of Green Metallurgy and Process Intensification, Ganzhou 341000, China

3) Jiangxi College of Applied Technology, Ganzhou 341000, China

4) Key Laboratory of Ionic Rare Earth Resources and Environment, Ministry of Natural Resources, Ganzhou 341000, China

(Received: 1 March 2021; revised: 28 April 2021; accepted: 29 April 2021)

**Abstract:** The effective recycling of waste printed circuit boards (WPCBs) can conserve resources and reduce environmental pollution. This study explores the pyrolysis and combustion characteristics of WPCBs in various atmospheres through thermogravimetric and Gaussian fitting analyses. Furthermore, this study analyses the pyrolysis products and combustion processes of WPCBs through thermogravimetric and Fourier transform infrared analyses (TG–FTIR) and thermogravimetry–mass spectrometry (TG–MS). Results show that the pyrolysis and combustion processes of WPCBs do not constitute a single reaction, but rather an overlap of multiple reactions. The pyrolysis and combustion process of WPCBs is divided into multiple reactions by Gaussian peak fitting. The kinetic parameters of each reaction are obtained by the Coats–Redfern method. In an argon atmosphere, pyrolysis consists of the overlap of the preliminary pyrolysis of epoxy resin, pyrolysis of small organic molecules, and pyrolysis of brominated flame retardants. The thermal decomposition process in the O<sub>2</sub> atmosphere is mainly divided into two reactions: brominated flame retardant combustion and epoxy combustion. This study provided the theoretical basis for pollution control, process optimization, and reactor design of WPCBs pyrolysis.

**Keywords:** waste printed circuit board; pyrolysis mechanism; combustion; Gauss; peak fitting


### 1. Introduction

Waste printed circuit boards (WPCBs) mainly contained metal, glass fiber, and organic matter, accounting for 40wt%, 30wt%, and 30wt%, respectively. It is a solid waste that can be used to recover metals and organics [1–6]. WPCBs recovery technologies include mechanical and physical treatment technology, heat treatment technology, hydrometallurgy technology, biological treatment technology, and pyrometallurgy technology [7–14]. At present, most of the WPCBs in the world are processed by pyrometallurgical technology, because it has strong adaptability to various raw materials and high metal yield [15]. It is worth noting that when WPCBs are burned at high temperature, the combustion of organic matter can provide additional heat when the furnace temperature exceeds 1000°C under certain reducing atmosphere in the smelting process. In addition, mineral components such as glass fiber can be used as fluxing agent to help to supply a certain amount of fluxing agent. Therefore, through smelting [16], copper products with high purity and high precious metal content can be obtained. The pyrometallurgical technology with high temperature combustion characteristics has the most potential and is an effective method. Therefore, the recycling of WPCBs resources is an important development direction [17–19].

WPCBs contain a variety of organic compounds. Organic matters are decomposed from the top in the feeding process of pyrometallurgy, and the temperature of flue gas generated can reach 1300°C. Most of the heat generated does not enter the melting pool, but is brought out by the flue gas, and the heat is not fully utilized. In addition, the decomposition of brominated organics can produce pollutants if the high temperature process is not properly controlled. Therefore, it is necessary to analyze the thermal decomposition characteristics of WPCBs during pyrolysis.

Many scholars have carried out pyrolysis experiments under different conditions to study the pyrolysis characteristics of WPCBs. Research has focused on the pyrolysis rate of WPCBs, the composition of pyrolysis oil, and the distribution of bromine in pyrolysis products and has obtained some results [20–24]. The kinetics of WPCBs from computer monitors and CPUs were studied by Rajagopal [25]. They considered that the pyrolysis of WPCBs in an inert atmosphere was a first-order reaction, and the activation energies calculated by the one-step integration method were 50.96–59.59 kJ/mol and 78.60–99.08 kJ/mol, respectively.

The composition of WPCBs is complex, it contains a large amount of metal, epoxy resin, bromine flame retardant, and other substances. The thermal decomposition process of waste printed circuit boards is not a single reaction [26]. Most

 Corresponding authors: Zhifeng Xu E-mail: xzf\_1@163.com; Jindi Huang E-mail: hjd041@163.com

© University of Science and Technology Beijing 2022

of the current studies regard the pyrolysis process of WPCBs as an overall reaction to obtain its mechanism function, which cannot well explain the entire pyrolysis process of WPCBs. At present, detailed research on the mechanism of this complex process is lacking. Therefore, it is necessary to conduct a detailed study on the thermal decomposition mechanism of WPCBs and explore its specific thermal decomposition mechanism. To further analyze the thermal decomposition process of WPCBs, the thermal decomposition products of WPCBs were analysed by thermogravimetric–Fourier transform infrared (TG–FTIR) and thermogravimetric–mass spectrometry (TG–MS). The decomposition mechanism of each reaction was studied by Gaussian fitting and the Coats–Redern (C-R) method. The research results provide guidance for the selection of combustion temperature and the control of pyrolysis, as well as the identification of combustion products and the reaction process of WPCBs. At the same time, this study provides a basic theory for modifying

the structure of the reactor and utilizing the heat energy generated by the combustion of organic matter in WPCBs.

## 2. Experimental

### 2.1. Raw materials

WPCBs substrate used for the experiment was provided by a waste electrical and electronic equipment (WEEE) treatment company in Shanghai, China. First, the electronic components on WPCBs were removed, and WPCBs were broken into blocks, crushed to a particle size of less than 0.15 mm by a pulveriser, and dried in an oven at 80°C for 48 h to remove the moisture in the circuit board powder. Finally, the circuit board powder was placed in a reactor for the pyrolysis combustion experiment (Fig. 1). The main components of the treated circuit board powder were metal, epoxy resin, and brominated flame retardants.

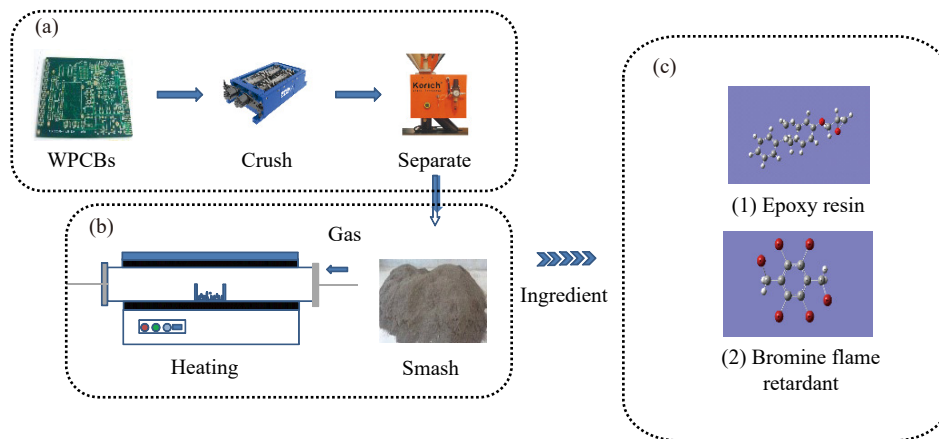


**Fig. 1.** Experimental procedure of the pyrolysis and combustion of WPCBs: (a) preprocessing of WPCB; (b) thermal decomposition process of WPCB; (c) composition of organic matter in WPCB.

### 2.2. TG experiment

The pyrolysis and combustion of WPCBs at different heating rates and in different atmospheres were analysed by using a simultaneous thermal analyser (STA449F5, Netzsch, Germany). The heating rates were 2, 5, and 8°C/min. The carrier gas was high-purity argon (Ar) and oxygen (O<sub>2</sub>). The flow rate was 20 mL/min.

To effectively determine the pyrolysis products of WPCBs, we set the heating rate to 5°C/min for infrared spectroscopy and mass spectrometry analyses. The pyrolysis process and products of WPCBs were analysed by using a pyrolysis-infrared ray light analyser. WPCBs were heated from 35–900°C at a heating rate of 5°C/min in a 20 mL/min Ar flow. The FTIR absorption band was in the range of 500–4000 cm<sup>-1</sup> with a detection resolution of 4 cm<sup>-1</sup>. A total of 16 scans were performed. The pyrolysis products of WPCBs were analysed by TG–MS at various temperatures of 35–900°C at a heating rate of 5°C/min.

### 2.3. Kinetic analysis

According to the theory of non-isothermal kinetics

[27–32], the rate equations of the thermal decomposition of solid substances under linear heating conditions are as follows:

$$\frac{d\alpha}{dt} = k(T) f(c) \quad (1)$$

$$\frac{d\alpha}{dT} = \frac{1}{\beta} k(T) f(\alpha) \quad (2)$$

where  $t$  is the time,  $T$  is the temperature,  $\beta$  is the heating rate,  $\alpha$  is the conversion percentage,  $\alpha = (m_0 - m_t)/(m_0 - m_\infty)$ ,  $m$  is the mass at different time periods,  $d\alpha/dT$  is the conversion rate of the reaction,  $k(T)$  is the temperature dependence of the rate constant,  $f(c)$  and  $f(\alpha)$  is the reaction mechanism function.

The temperature dependence of the rate constant ( $k(T)$ ) is in accordance with the Arrhenius law [33]:

$$k(T) = A \exp\left(-\frac{E}{RT}\right) \quad (3)$$

where  $A$  is the pre-exponential factor,  $E$  is the activation energy,  $R$  is the molar gas constant, and  $T$  is the thermodynamic temperature.

By substituting Eq. (3) into Eq. (2), Eq. (4) can be obtained:

$$\frac{d\alpha}{dT} = \frac{A}{\beta} \exp\left(-\frac{E}{RT}\right) f(\alpha) \quad (4)$$

The  $f(\alpha)$  of a simple reaction can be defined by  $f(\alpha) = (1 - \alpha)^n$ , thereby providing the following:

$$\frac{d\alpha}{dt} = kf(\alpha) = k_0 \exp\left(-\frac{E}{RT}\right) (1 - \alpha)^n \quad (5)$$

where  $k$  is the rate constant, and  $k_0$  is the isokinetic rate constant.

The activation energy of the entire reaction was determined by the Kissinger–Akah–Sunose (KAS), Flynn–Wall–Ozawa (FWO) and Friedman–Reich–Levi (FRL) methods [34]. Then, the Coats–Redfern method was used to obtain the pyrolysis mechanism function of WPCBs.

The KAS model method is based on the following equations:

$$\ln\left(\frac{\beta}{T}\right) = \ln\left[\frac{AR}{EG(\alpha)}\right] - \frac{E}{RT} \quad (6)$$

where  $G(\alpha)$  is the integral mechanism function.

The activation energy rates of the different conversions can be calculated by the linear relationship between  $\ln(\beta/T)$  and  $1/T$ .

The FWO model method is based on the following equations:

$$\ln \beta = \lg\left[\frac{AE}{RG(\alpha)}\right] - 2.315 - 0.4567 \frac{E}{RT} \quad (7)$$

The activation energy rates of the different conversions can be calculated by the linear relationship between  $\ln \beta$  and  $1/T$ .

The FRL model is based on the following equations:

$$\ln\left(\frac{\beta d\alpha}{dT}\right) = \ln[Af(\alpha)] - \frac{E}{RT} \quad (8)$$

We draw the graph from  $\ln((\beta d\alpha)/(dT))$  to  $1/T$  to fit the data with the least squares method, thus calculating  $E$  with the slope and  $A$  with the intercept.

The Coats–Redfern model (C-R) is expressed as follows [35–36]:

We subject Eq. (6) to variable separation and integrate the change to obtain the following:

$$\ln\left[\frac{G(\alpha)}{T^2}\right] = \ln\left[\frac{AR}{\beta E}\left(1 - \frac{2RT}{E}\right)\right] - \frac{E}{RT} \quad (9)$$

For most of the reactions,  $E/(RT) \gg 1$  and  $1 - RT/E \approx 1$  during the heating process. Thus, we draw the graph from  $\ln((\beta d\alpha)/(dT))$  to  $1/T$ , with a slope of  $-E/(RT)$ .

## 2.4. Gaussian fitting analysis

Regarding the kinetic analysis of complex processes with overlapping reactions, an effective method is to fit each peak into a quantity of reactions by using a statistical function and then to obtain the kinetic parameters through the analysis of each fitted peak [37]. Gaussian fitting analysis refers to decomposing a complex curve into several Gaussian fit peaks

according to the Gaussian function rule. This method can greatly simplify the numerical calculation model while ensuring the accuracy of the solution, and has good applicability. The Gaussian peak fitting method is mostly used in spectral analysis and numerical analysis, and it is widely used in physical chemistry experiments. Due to the simplicity and applicability of Gaussian peak fitting, it has been gradually applied to some complicated pyrolysis reactions, and it can well reflect the changing law of pyrolysis processes [38–39]. The principle of Gaussian fitting is expressed as follows [40].

We let a discrete set of experimental data  $(x_i, y_i)$  ( $i = 1, 2, \dots, n$ ) be expressed as a Gaussian function:

$$y_i = y \exp\left[\frac{-(x_i - x_{\max})^2}{s}\right] \quad (10)$$

where  $s$  represents half the peak width, and  $x_{\max}$  is the maximum value of  $x$ .

We take the natural logarithm on both sides of Eq. (3) and convert it into Eq. (11):

$$\ln y_i = \ln y \exp\left[\frac{-(x_i - x_{\max})^2}{s}\right] \quad (11)$$

$$\ln y_i = \left(\ln y_{\max} - \frac{x_{\max}^2}{s}\right) + 2 \frac{x_i x_{\max}}{s} - \frac{x_i^2}{s} \quad (12)$$

Order

$$\ln y_i = a_i, \ln y_{\max} - \frac{x_{\max}^2}{s} = b_0, \frac{x_i x_{\max}}{s} = b_1, -\frac{1}{s} = b_2 \quad (13)$$

It is converted in a quadratic polynomial fitting function:

$$a_i = b_0 + b_1 + b_2 = \begin{pmatrix} 1, x_i, x_i^2 \end{pmatrix} \begin{bmatrix} b_0 \\ b_1 \\ b_2 \end{bmatrix} \quad (14)$$

which can be expressed in matrix form:

$$\begin{bmatrix} z_1 \\ z_2 \\ \vdots \\ z_n \end{bmatrix} = \begin{bmatrix} 1 & x_1 & x_1^2 \\ \vdots & \vdots & \vdots \\ 1 & x_n & x_n^2 \end{bmatrix} \begin{bmatrix} b_0 \\ b_1 \\ b_2 \end{bmatrix} \quad (15)$$

It can be expressed as:

$$\mathbf{Z}_{n \times 1} = \mathbf{X}_{n \times 3} \mathbf{B}_{3 \times 1} \quad (16)$$

According to the least squares method, the generalized least squares solution of matrix  $\mathbf{B}$  formed by the fitting constants  $b_0$ ,  $b_1$ , and  $b_2$  is shown in Eq. (17).

$$\mathbf{B} = (\mathbf{X}^T \mathbf{X})^{-1} \mathbf{X}^T \mathbf{Z} \quad (17)$$

Thus, the parameters  $y_{\max}$ ,  $x_{\max}$ , and  $s$  that need to be estimated, can be solved, and the Gaussian fitting curve of the data set can be obtained.

For these simultaneous complex reactions, the  $d\alpha/dT$  curve can be fitted by the following formula to obtain the fitting function of each fitting reaction [41]:

$$y = y_0 + \sum_{i=1}^n \left[ \frac{A_i}{\omega_i \sqrt{\frac{\pi}{2}}} \exp\left(-2 \frac{x - x_{c_i}}{\omega_i^2}\right) \right] \quad (18)$$

where  $i = 1, 2, 3, \dots, n$ ;  $y_0$  is the baseline;  $A_i$  is the fitted peak area;  $\omega_i$  is the half-height width of the fitting peak; and  $x_{c_i}$  is the transverse position of the fit peak.

### 3. Results and discussion

#### 3.1. Effect of the heating rate on the pyrolysis and combustion behaviour of WPCBs

To investigate the pyrolysis and combustion mechanism of WPCBs, we studied the thermogravimetric (TG) and derivative thermogravimetric (DTG) curves of pyrolysis and combustion at different heating rates and in different atmospheres by using a comprehensive TG analyser. The results are shown in Fig. 2. Fig. 2(a) shows the TG and DTG curves of WPCBs in an Ar atmosphere, and Fig. 2(b) presents the TG and DTG curves of WPCBs in an O<sub>2</sub> atmosphere. The TG and DTG curves gradually shifted to higher temperature as the heating rate increased. This phenomenon was mainly due to the increase in the heating rate, which led to thermal conduction lag and untimely gas diffusion. The increase in

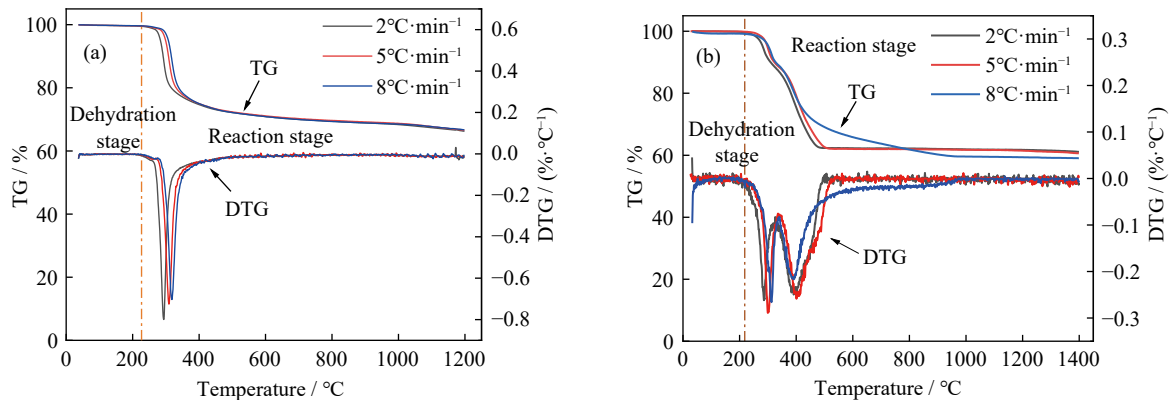


Fig. 2. TG curves of the pyrolysis combustion of WPCBs in (a) Ar and (b) O<sub>2</sub> atmospheres.

#### 3.2. Effect of the gas atmosphere on the pyrolysis and combustion of WPCBs substrates

##### 3.2.1. Pyrolysis characteristics of WPCBs substrates in an Ar atmosphere

As shown in Fig. 2(a), the mass-loss rate during the pyrolysis of WPCBs in an Ar atmosphere was approximately 32%; this mass loss could be divided into two stages: dehydration and main pyrolysis. The temperature range of the dehydration stage was 30–150°C, which was mainly due to the volatilization of water in WPCBs. In the material used in this study, after drying, the loss of water was not obvious in the pyrolysis process, and the mass loss due to water was only 1%. The temperature range of the main pyrolysis stage was 230–680°C, which was the main mass-loss stage of WPCBs pyrolysis process. Small-molecule gases and volatile compounds were mainly generated from the pyrolysis of WPCBs, and the mass loss was 31%. Based on considering the 5°C/min heating rate curve as an example, the pyrolysis rate of WPCBs increased as the temperature increased in the main pyrolysis stage to reach the maximum at 308°C; thus, the mass-loss rate was approximately 3.6%/min.

##### 3.2.2. Combustion characteristics of WPCBs substrate in an O<sub>2</sub> atmosphere

The TG and DTG curves of WPCBs in an O<sub>2</sub> atmosphere are presented in Fig. 2(b). In an O<sub>2</sub> atmosphere, the mass-loss

rate of WPCBs was approximately 38%, and its characteristic combustion curve could be divided into three mass-loss stages. Taking the TG curve at a 5°C/min heating rate as an example, the first mass-loss stage of WPCBs in the O<sub>2</sub> atmosphere was mainly water volatilization; the temperature range at this stage was 30–150°C, and the mass-loss rate was 1%. In the second stage, the mass-loss rate increased as the temperature increased from 200–338°C. The mass-loss rate reached the maximum of 1.45%/min at 300°C, and then decreased with increasing temperature. The temperature range of the third mass-loss stage was 338–530°C, during which the mass-loss rate increased gradually with increasing temperature until reaching a maximum value of 1.25%/min at 400°C. Thereafter, the mass-loss rate gradually decreased until the end of the reaction.

In an O<sub>2</sub> atmosphere, the organic compounds in WPCBs could be fully combusted to produce various types of volatile gases; thus, its mass-loss rate was higher than that in the Ar atmosphere. In the Ar atmosphere, WPCBs reacted violently in the main pyrolysis region, and the maximum mass-loss rate was much higher than that in the O<sub>2</sub> atmosphere.

#### 3.3. Analysis of the gas products in different atmospheres

##### 3.3.1. Gas products from pyrolysis in an Ar atmosphere

The pyrolysis products of WPCBs in an Ar atmosphere

the heating rate decreased the time to reach the final temperature, and the temperature difference between the interior and exterior of the particle increased, thereby leading to thermal hysteresis. When the heating rate was high, the generation rate of pyrolysis products increased, and the gas products could not overflow in time; this result led to curve hysteresis and caused the TG curve to shift to the right [42]. In an Ar atmosphere, the thermal decomposition reaction of WPCBs occurred at 230–680°C. In this temperature range, the epoxy resin and bromine flame retardant decomposed rapidly, resulting in the DTG curves overlapping and showing a peak. In the O<sub>2</sub> atmosphere, the epoxy resin in WPCBs first decomposed, the bromine flame retardant decomposed, and the two reactions occurred in different temperature ranges and at maximum mass loss rate temperatures, resulting in the partial overlap of DTG curves; two peaks appeared in the whole DTG curves.

##### 3.3.1. Gas products from pyrolysis in an Ar atmosphere

The pyrolysis products of WPCBs in an Ar atmosphere

were analysed by TG–FTIR, and the results are shown in Fig. 3(a). According to Fig. 3(a), when the temperature was lower than 200°C, only a small adsorption peak appeared in the FTIR spectrum. An intense thermal decomposition reaction does not occur at 200°C. When the temperature was higher than 300°C, a mass of absorption peaks appeared in the FTIR spectra. At this time, an intense pyrolysis reaction occurs and a large number of pyrolysis products are produced. Strong

adsorption peaks at 2500–2700  $\text{cm}^{-1}$  and 1400–1600  $\text{cm}^{-1}$  were observed due to the tensile vibration of H–Br and the frame vibration of benzene rings, respectively, due to the thermal decomposition of the bromine-containing organic substances in the circuit board substrate, which forms HBr [43]. The strong adsorption peak at 2240–2400  $\text{cm}^{-1}$  was mainly due to the stretching vibration of the C=O bond of  $\text{CO}_2$  [44]. The stretching vibration peak of –OH was detected

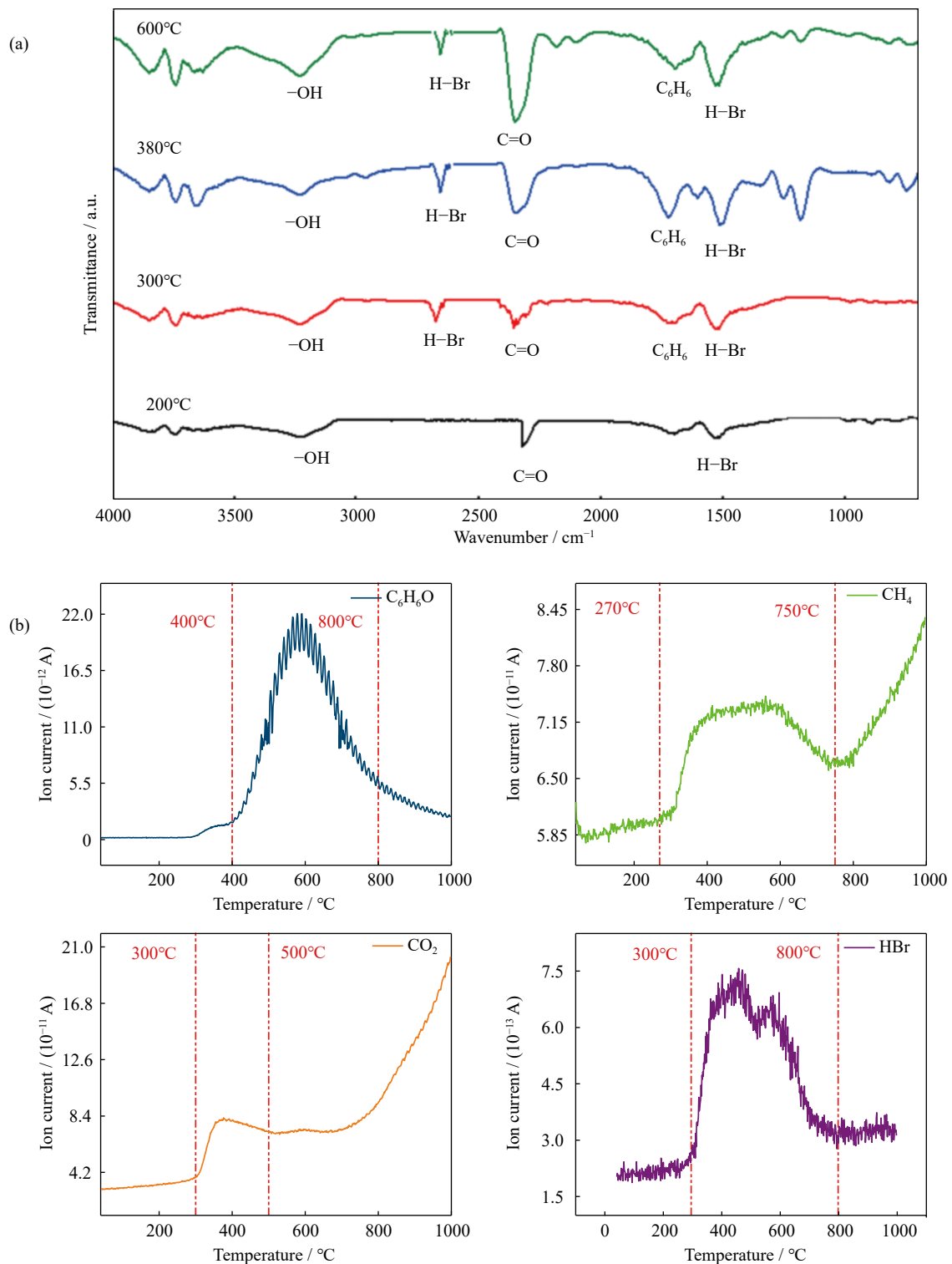


Fig. 3. Analysis of pyrolysis products obtained in the Ar atmosphere with a heating rate of 5°C/min: (a) TG–FTIR analysis; (b) TG–MS analysis.



at 3100–3500  $\text{cm}^{-1}$ , which was mainly due to the stretching vibrations of the hydroxy and phenolic hydroxyl groups [45].

The main pyrolytic products of WPCBs and their relative intensities in an Ar atmosphere were measured by TG–MS. The results are presented in Fig. 3(b). As shown in Fig. 3(b), the pyrolysis of WPCBs in an Ar atmosphere mainly generated polymers, such as phenol and bromophenol, and gases, such as  $\text{CH}_4$ ,  $\text{C}_2\text{H}_2$ , HBr,  $\text{H}_2\text{O}$ , and  $\text{CO}_2$ . The peaks of  $\text{C}_6\text{H}_6\text{O}$  and HBr are detected at 300–800°C. These substances are mainly produced continuously in one stage. This is mainly due to the decomposition reaction of the bromine flame retardant in WPCBs to release Br. Amount of small hydrocarbon molecules, such as  $\text{CH}_4$ ,  $\text{C}_2\text{H}_2$ , CO, and  $\text{CO}_2$ , were detected from 300–750°C, which was mainly due to the initial pyrolysis of the epoxy resin in WPCBs. As the temperature increased, the remaining small molecular polymers further pyrolysed to produce a large amount of  $\text{CO}_2$  and  $\text{H}_2\text{O}$ . Owing to the delay between pyrolysis and mass spectrometry detection, the temperature range of product formation detected by TG–MS was higher than the actual pyrolysis temperature. In addition, the heating process was continuous, which also led to the overlap of various reaction products.

According to the analysis results of TG–FTIR and TG–MS, the pyrolysis process of WPCBs in an Ar atmosphere was the overlap of three reactions: preliminary pyrolysis of epoxy resin, pyrolysis of bromine flame retardant, and pyrolysis of organic small molecules. With the increase of temperature, the bromine flame retardant in WPCBs begins to depolymerize to produce benzene, phenol, HBr, and other substances. The epoxy resin also began to decompose to produce small organic molecules,  $\text{CO}_2$ ,  $\text{H}_2\text{O}$ , and other substances. As the temperature rises further, the organic small molecule compounds are gradually decomposed.

### 3.3.2. Gas products from combustion in an $\text{O}_2$ atmosphere

To analyse the combustion mechanism of WPCBs in  $\text{O}_2$ , we conducted TG–FTIR and TG–MS. In this study, TG–FTIR was used to investigate the chemical bonds and functional groups in the pyrolysis products, and TG–MS was used to analyse the formation process of the main components in the pyrolysis products. Fig. 4(a) presents the infrared spectra of gas products from the combustion of WPCBs in an  $\text{O}_2$  atmosphere at different temperatures. With increasing temperature, the deformation vibration peak and stretching vibration peak of C=O were observed at 667 and 2360  $\text{cm}^{-1}$ , respectively. Strong adsorption peaks were observed at 2500–2600  $\text{cm}^{-1}$  and 1400–1600  $\text{cm}^{-1}$ , which were attributed to the stretching vibration of HBr and frame vibration of the benzene ring, respectively. The absorption band detected at 2100–2270  $\text{cm}^{-1}$  was due to the stretching vibrations of C=C. Absorption peaks could be observed at 2100–2140  $\text{cm}^{-1}$  and 2150–2260  $\text{cm}^{-1}$ , which represented the stretching vibration peaks of the C=C bond. At 3530–3650  $\text{cm}^{-1}$  and 3650–3780  $\text{cm}^{-1}$ , the characteristic absorption peaks of –OH were detected, which were mainly due to the stretching vibrations of the hydroxy and phenolic hydroxyl groups.

The combustion products of WPCBs and their relative in-

tensities in the  $\text{O}_2$  atmosphere were measured by TG–MS, and the results are shown in Fig. 4(b). According to Fig. 4(b), from 250–600°C, peaks of  $\text{C}_6\text{H}_6$ ,  $\text{H}_2\text{O}$ ,  $\text{CO}_2$ , and HBr was observed, and the yields of benzene, a benzene homologue, and HBr increased with increasing temperature before reaching a peak at 450°C. This result was mainly due to the combustion of brominated flame retardants in WPCBs; thus, this condition was the main release stage of bromine in WPCBs. From 250 to 900°C, a mass of small hydrocarbon molecules, such as  $\text{CH}_4$ ,  $\text{C}_2\text{H}_4$ ,  $\text{C}_2\text{H}_6$ , as well as CO and  $\text{CO}_2$ , were detected, indicating that the epoxy resin in WPCBs began to combust in the  $\text{O}_2$  atmosphere. Owing to the delay of pyrolysis and mass spectrometry detection, the temperature range of product formation detected by TG–MS was higher than the actual pyrolysis temperature.

According to the results of the TG–FTIR and TG–MS analyses, the combustion of WPCBs in an  $\text{O}_2$  atmosphere could be divided into two reactions: brominated flame retardant combustion and epoxy combustion. In the  $\text{O}_2$  atmosphere, the brominated flame retardants in WPCBs first began to burn with increasing temperature, thereby producing a large amount of benzene phenol, benzene homologues, and HBr. This condition was the main release stage of bromine from WPCBs. Then, the epoxy resin in WPCBs combusted to produce  $\text{CH}_4$ ,  $\text{C}_2\text{H}_8$ , CO,  $\text{CO}_2$ ,  $\text{H}_2\text{O}$ , and other substances.

The gas products of pyrolysis and combustion in the Ar and  $\text{O}_2$  atmospheres were considerably different. In the Ar atmosphere, WPCBs pyrolysis produced hydrocarbons, phenol, CO,  $\text{CO}_2$ , and other substances. In the  $\text{O}_2$  atmosphere, the organic matter in WPCBs could be fully burned, thereby producing  $\text{CO}_2$ ,  $\text{H}_2\text{O}$ , and other substances.

## 3.4. Mechanism models

### 3.4.1. Mechanism model in an Ar atmosphere

The pyrolysis process of WPCBs was analysed using the iso-conversion methods of KAS, FWO, and FRL. The obtained reaction activation energy is shown in Fig. 5. The activation energy of the pyrolysis of WPCBs was unstable and changed as the reaction progressed. The activation energy of the pyrolysis of WPCBs was approximately 145 kJ/mol when  $\alpha$  was between 0 and 0.6, and it increased to 270 kJ/mol when  $\alpha$  was 0.9. The main reason for this, as explained earlier, was that the pyrolysis of WPCBs was not a single reaction but the overlap of multiple reactions [46].

According to the Gaussian peak fitting rule [47], the peak fitting of the WPCBs pyrolysis process was decomposed into three reactions. Using  $\beta = 5^\circ\text{C}/\text{min}$  as the fitting object, the pyrolysis process was fitted with First Optimization (1stOpt) fitting optimization software and the general global optimization algorithm. The fitting coefficient reached 0.998, and the result is shown in Fig. 6. The mass-loss phase of WPCBs could be fitted by three fitting peaks.

According to the results of Gaussian peak fitting, the main parameters of the fitting peaks are counted and listed in Table 1. From the TG curve, DTG curve, and pyrolysis products of WPCBs, we could observe only one main mass-

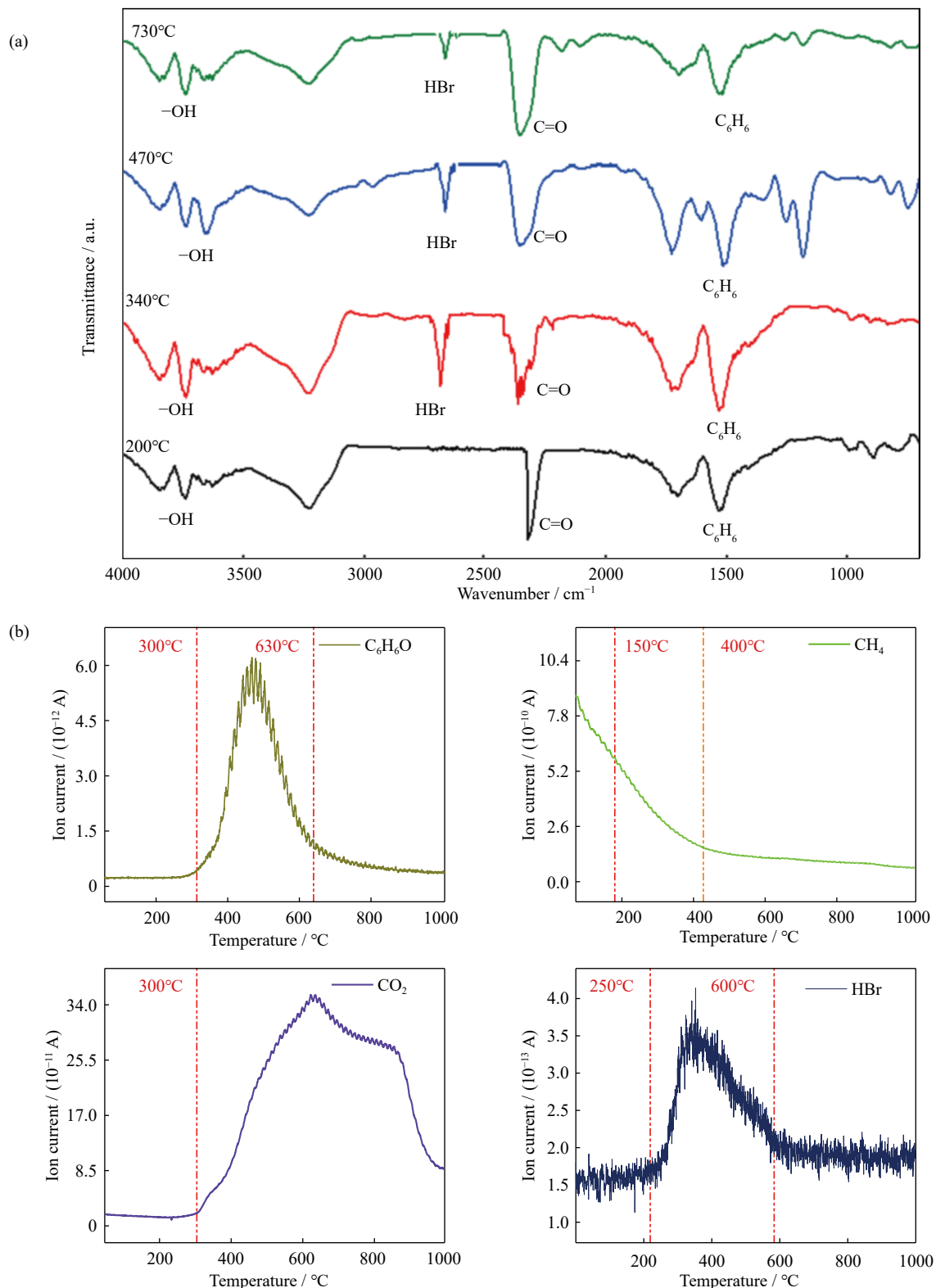


Fig. 4. Analysis of pyrolysis products obtained in the  $\text{O}_2$  atmosphere with a heating rate of  $5^\circ\text{C}/\text{min}$ : (a) TG-FTIR analysis; (b) TG-MS analysis.

loss stage in the pyrolysis process. However, the reaction was more complex and required three fitting peaks. Fitting peak 1 attributed to the mass loss of WPCBs was from 250 to  $450^\circ\text{C}$ , and the maximum mass-loss temperature was  $330^\circ\text{C}$ . At this stage, brominated flame retardants were pyrolysed to form HBr and other substances. The mass-loss range of fitting peak 2 was  $280\text{--}350^\circ\text{C}$ , and the maximum mass-loss

temperature was  $320^\circ\text{C}$ . At this stage, epoxy resin was pyrolysed into a small-molecule polymer. The mass-loss range of fitting peak 3 was  $250\text{--}700^\circ\text{C}$ , and the maximum mass-loss temperature was  $450^\circ\text{C}$ . At this stage, organic small-molecular compounds were mainly pyrolysed into  $\text{CO}$ ,  $\text{CO}_2$ ,  $\text{H}_2\text{O}$ , and other substances.

WPCBs substrate pyrolysis process was divided into three

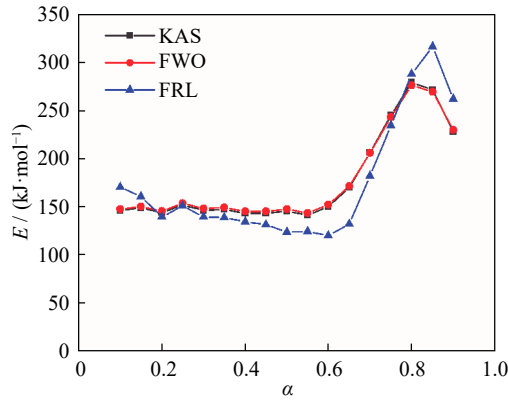


Fig. 5. Reaction activation energy obtained by the KAS, FWO, and FRL methods in Ar.

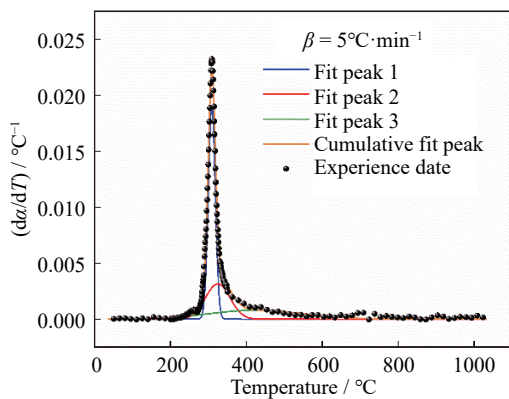


Fig. 6. Analysis results of Gaussian fitting for the Ar atmosphere.

Table 1. Fitting peak temperature interval in Ar

Fitting peak	Proportion / wt%	Initial temperature, $T_i / ^\circ\text{C}$	Peak temperature, $T_p / ^\circ\text{C}$	Termination temperature, $T_e / ^\circ\text{C}$
1	0.28	250	330	450
2	0.45	280	320	350
3	0.27	250	450	700

superimposed reactions by the Gaussian peak separation method, and the pyrolysis parameters were obtained by analysing the pyrolysis kinetics of the three reactions. To determine the pyrolysis mechanism function of WPCBs, we used the Malek method [48] to further differentiate the mechanism function. The standard curves of  $y(\alpha) = [f(\alpha) \times G(\alpha)] / [f(0.5) \times G(0.5)]$  and  $\alpha$  calculated on the basis of the mechanism functions are shown in Fig. 7 together with the curves of  $y(\alpha) = (T/T_{0.5})^2 \times (d\alpha/dt) / [(d\alpha/dt)_{0.5}]$  and  $\alpha$  calculated on the basis of the mass-loss curves. As shown in Fig. 7, in the pyrolysis process, the  $y(\alpha)$  results of the three fitting reactions all had an asymmetric parabolic shape. The function corresponding to the standard curve fitting the  $y(\alpha)$  test curve of the initial pyrolysis of epoxy resin was the reaction order, and the mechanism was a chemical reaction, with  $G(\alpha) = (1 - \alpha)^{-1} - 1$ . The  $E_0$  and  $k_0$  values for C-R during this process were 126.47 kJ/mol and  $2.9 \times 10^{10} \text{ s}^{-1}$ , respectively. The function corresponding to the standard curve fitting the  $y(\alpha)$  test curve of the thermal decomposition of bromine flame re-

tardant was the chemical reaction, with  $G(\alpha) = (1 - \alpha)^{-1} - 1$ . The  $E_0$  and  $k_0$  values for C-R during the process were 503.07 kJ/mol and  $2.0 \times 10^{44} \text{ s}^{-1}$ , respectively. The function corresponding to the standard curve fitting the  $y(\alpha)$  test curve of the thermal decomposition of organic small-molecular compounds was the Avrami–Erofeev equation. The mechanism was random nucleation and subsequent growth, and the reaction order was 4. The reaction mechanism function was  $G(\alpha) = [-(1 - \alpha)]^4$ . The  $E_0$  and  $k_0$  for C-R during the process were 137.25 kJ/mol and  $1.2 \times 10^7 \text{ s}^{-1}$ , respectively.

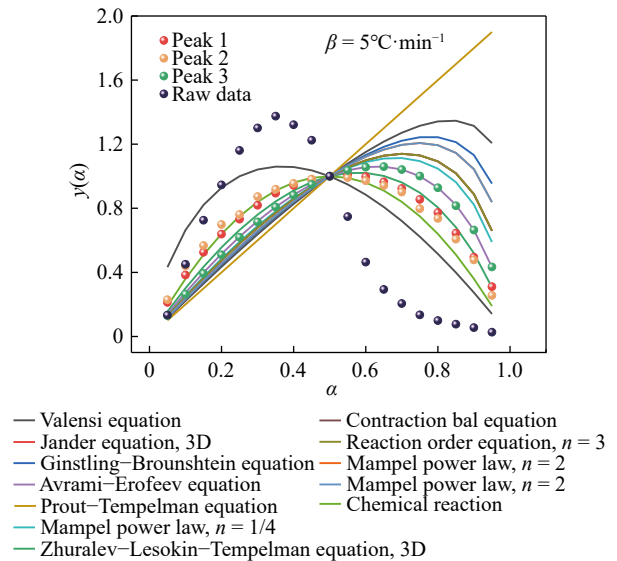


Fig. 7.  $y(\alpha)$  standard curve and test curve in the Ar atmosphere.

The conversion ( $\alpha$ ) curves at the heating rate of  $2^\circ\text{C}/\text{min}$  were calculated by the obtained kinetic parameters, and the reliability of the kinetic results was verified by comparison with the experimental data. The results are shown in Fig. 8. The predicted value obtained by the mechanism function was basically consistent with the actual value. Therefore, the above mechanism function could be used to predict the change in the pyrolysis conversion rate of WPCBs in Ar.

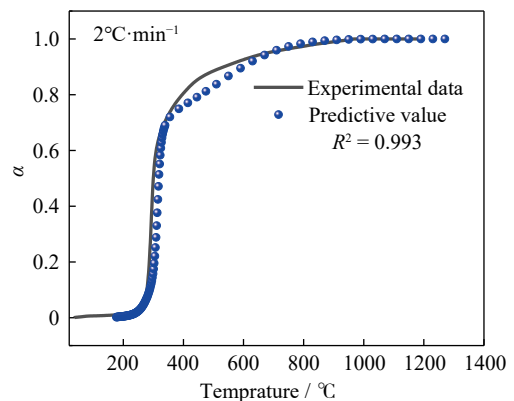


Fig. 8. Comparison of the experimental value to the predicted value at  $2^\circ\text{C}/\text{min}$  in Ar.

### 3.4.2. Mechanism model in an $\text{O}_2$ atmosphere

The activation energy of WPCBs combusting in  $\text{O}_2$  was obtained by the KAS, FWO, and FRL methods, and the res-



ults are presented in Fig. 9. The activation energy of WPCBs combustion in O<sub>2</sub> was not stable but changed with the progression of the reaction. When  $\alpha$  was in the 0–0.4 range, the activation energy of the reaction was approximately 180 kJ/mol. When  $\alpha$  was in the 0.4–0.7 range, the activation energy increased gradually to 300 kJ/mol. The activation energy decreased gradually to 50 kJ/mol in the range of 0.7–0.8. The main reason for this was that the composition of WPCBs substrate was relatively complex, but WPCBs substrate mainly contained epoxy resin and brominated flame retardants; therefore, its combustion in O<sub>2</sub> was not a single reaction but the overlap of multiple reactions, and the activation energy varied for different reactions.

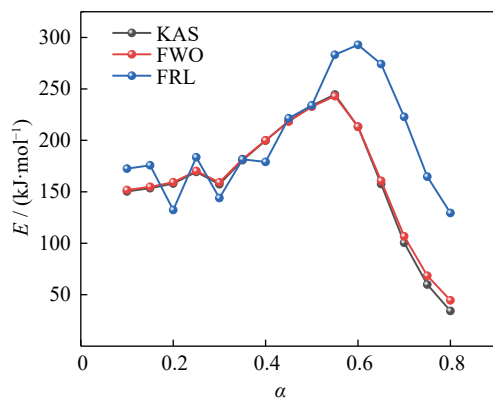


Fig. 9. Reaction activation energy obtained by the KAS, FWO, and FRL methods in O<sub>2</sub>.

To further analyse the mechanism of the combustion process, this study used the Gaussian peak fitting analysis method for reference. 1stOpt software was applied to divide the combustion of WPCBs into epoxy resin combustion curves and brominated flame retardant combustion curves. Taking the combustion curve at 5°C/min as an example, the fitting results are shown in Fig. 10 and Table 2. Fitting curve 1 represented the combustion curve of the brominated flame retardants. The combustion temperature was 250–360°C, and the main products were C<sub>6</sub>H<sub>6</sub>, C<sub>6</sub>H<sub>6</sub>O, HBr, CO<sub>2</sub>, and others. Fitting curve 2 was the combustion curve of the epoxy resin, and the combustion temperature was 250–600°C. Some small hydrocarbon molecules were produced along with a large amount of H<sub>2</sub>O, CO, CO<sub>2</sub>, and other substances.

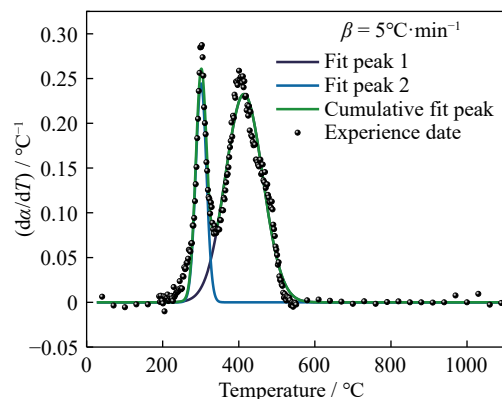


Fig. 10. Analysis results of Gaussian fitting for O<sub>2</sub> atmosphere.

Table 2. Fitting peak temperature interval in the O<sub>2</sub> atmosphere

Fitting peak	Proportion / wt%	Initial temperature, T <sub>i</sub> / °C	Peak temperature, T <sub>p</sub> / °C	Termination temperature, T <sub>e</sub> / °C
1	0.24	250	300	360
2	0.76	280	400	600

To further determine the combustion mechanism functions of the circuit board in O<sub>2</sub>, we used the Malek method to sift the mechanism functions. The standard curves of  $y(\alpha) = [f(\alpha) \times G(\alpha)] / [f(0.5) \times G(0.5)]$  and  $\alpha$  calculated on the basis of the mechanism functions are shown in Fig. 11 together with the curves of  $y(\alpha) = (T/T_{0.5})^2 \times (d\alpha/dt) / [(d\alpha/dt)_{0.5}]$  and  $\alpha$  calculated on the basis of the mass-loss curves. Fig. 11 shows two reactions of WPCBs fitted by the Malek method at a heating rate of 5°C/min. The figure indicated that the experimental curve of brominated flame retardant combustion (the reaction of peak 1) was closest to the curve of the Zhuravlev–Lesokin–Tempelman (Z-L-T) equation mechanism function  $y(\alpha)/y(\alpha)_{0.5}$ . The reaction mechanism function of brominated flame retardant combustion was  $G(\alpha) = [(1-\alpha)^{-1/3} - 1]^2$ . The  $E_0$  and  $k_0$  for C-R during the process were 563.7 kJ/mol and  $2.97 \times 10^{49} \text{ s}^{-1}$ , respectively. The figure showed that the experimental curve of epoxy resin combustion (fitting reaction 2) was closest to the function  $y(\alpha)/y(\alpha)_{0.5}$  function curve of the Z-L-T equation mechanism, with the function  $G(\alpha) = [(1-\alpha)^{-1/3} - 1]^2$ . The  $E_0$  and  $k_0$  for C-R during the process were 205.32 kJ/mol and  $2.99 \times 10^{13} \text{ s}^{-1}$ , respectively. The combustion reaction of WPCBs in O<sub>2</sub> indicated the overlap of two reactions. As the temperature increased, the HBr and phenol homologues in WPCBs began to combust, and as the temperature further increased, the resin in WPCBs began to burn.

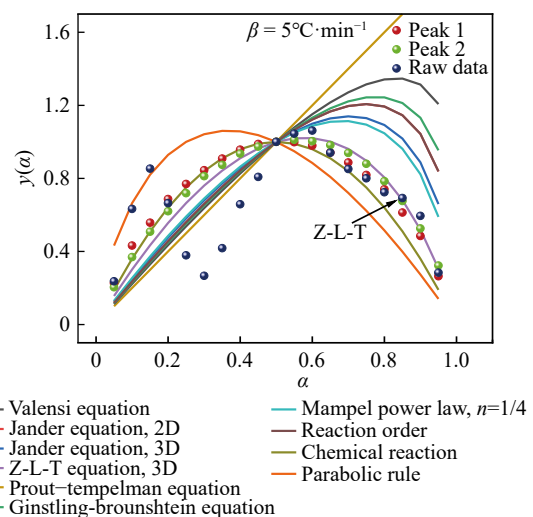


Fig. 11.  $y(\alpha)$  standard curve and test curve in the O<sub>2</sub> atmosphere.

The conversion curves at the heating rate of 2°C/min were calculated by the obtained kinetic parameters, and the reliability of the kinetic results was verified by comparison with the experimental data. The results are shown in Fig. 12. The pre-

dicted value obtained by the mechanism function was basically consistent with the actual value. Therefore, it could be proven that the above mechanism function could be used to predict the change in the pyrolysis conversion rate of WPCBs in O<sub>2</sub>.

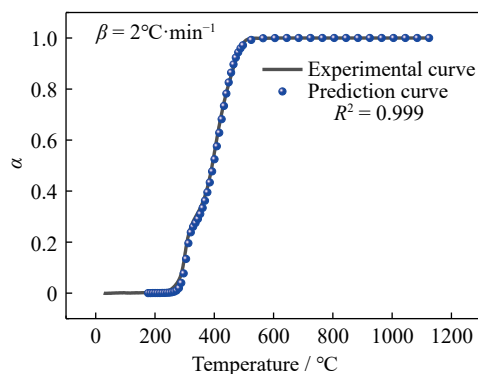


Fig. 12. Comparison of the experimental value to the predicted value of the conversion ( $\alpha$ ) at 2°C/min in O<sub>2</sub>.

#### 4. Conclusion

In an Ar atmosphere, the temperature range of pyrolysis was 260–680°C, and the mass loss was 32%. The thermal decomposition process in the Ar atmosphere is mainly divided into three reactions: the preliminary pyrolysis of epoxy resin, pyrolysis of bromine flame retardant, and pyrolysis of small organic molecules. The bromine flame retardant thermally decomposes at 250–450°C to generate phenol, HBr, and other substances. The reaction mechanism is a chemical reaction model, and the reaction activation energy is 503.07 kJ/mol. The epoxy resin decomposes at 280–350°C to generate small organic molecules, CO<sub>2</sub>, and H<sub>2</sub>O. The reaction mechanism is a chemical reaction, and the reaction activation energy is 126.47 kJ/mol. At 250–700°C, small organic molecules decompose to form CO<sub>2</sub>, H<sub>2</sub>O, and other substances. The reaction mechanism is Avrami–Erofeev equation, and the reaction activation energy is 137.25 kJ/mol.

In an O<sub>2</sub> atmosphere, the combustion temperature range was 230–520°C, and the mass loss was 40%. The thermal decomposition process in the O<sub>2</sub> atmosphere is mainly divided into two reactions: brominated flame retardant combustion and epoxy combustion. Bromine flame retardants in WPCBs burn at 250–360°C to generate phenol, HBr, and other substances. The reaction mechanism is Z-L-T equation, and the reaction activation energy is 563.7 kJ/mol. At 280–600°C, the epoxy resin in WPCBs will undergo a combustion reaction to generate CO<sub>2</sub>, H<sub>2</sub>O, and other substances. The reaction mechanism is Z-L-T equation, and the reaction activation energy is 205.32 kJ/mol.

#### Acknowledgements

This work was financially supported by the National Key R&D Program of China (Nos. 2019YFC1908400 and 2019YFC1907405), the National Natural Science Founda-

tion of China (Nos. 51904124, 51804139, 52004111 and 52074136), the Jiangxi Provincial Cultivation Program for Academic and Technical Leaders of Major Subjects (Nos. 20212BCJL23052 and 20212BCJ23007), the Distinguished Professor Program of Jinggang Scholars, China Institutions of Higher Learning Jiangxi Province, the Science and Technology Research Project of the Jiangxi Provincial Department of Education (No. gjj170507), and the Science Research Foundation of Jiangxi University of Science and Technology (No. jxxjbs 17046).

#### Conflict of Interest

The authors have no competing interests to declare that are relevant to the content of this article.

#### References

- [1] Y.C. He and Z.M. Xu, Recycling gold and copper from waste printed circuit boards using chlorination process, *RSC Adv.*, 5(2015), No. 12, p. 8957.
- [2] J.B. Wang, J. Guo, and Z.M. Xu, An environmentally friendly technology of disassembling electronic components from waste printed circuit boards, *Waste Manage.*, 53(2016), p. 218.
- [3] Z. Sun, Y.P. Xiao, H. Agterhuis, J. Sietsma, and Y.X. Yang, Recycling of metals from urban mines - a strategic evaluation, *J. Clean. Prod.*, 112(2016), p. 2977.
- [4] J.W. Li, X. Han, R.X. Chai, F.Q. Cheng, M. Zhang, and M. Guo, Metal-doped (Cu,Zn)Fe<sub>2</sub>O<sub>4</sub> from integral utilization of toxic Zn-containing electric arc furnace dust: An environment-friendly heterogeneous Fenton-like catalyst, *Int. J. Miner. Metall. Mater.*, 27(2020), No. 7, p. 996.
- [5] L. Xiao, P.W. Han, Y.L. Wang, G.Y. Fu, Z. Sun, and S.F. Ye, Silver dissolution in a novel leaching system: Reaction kinetics study, *Int. J. Miner. Metall. Mater.*, 26(2019), No. 2, p. 168.
- [6] Z.L. Liu, Z.H. Zhang, Z.L. Li, X.F. Xie, S.P. Zhong, Y.H. Li, Z.F. Xu, and H. Liu, 3D hierarchical iron-cobalt sulfide anchored on carbon fiber with abundant active short chain sulfur for high-efficiency capture of elemental mercury, *Chem. Eng. J.*, 418(2021), art. No. 129442.
- [7] L. Flandinet, F. Tedjar, V. Ghetta, and J. Fouletier, Metals recovering from waste printed circuit boards (WPCBs) using molten salts, *J. Hazard. Mater.*, 213-214(2012), p. 485.
- [8] G.B. Liang, J.H. Tang, W.P. Liu, and Q.F. Zhou, Optimizing mixed culture of two acidophiles to improve copper recovery from printed circuit boards (PCBs), *J. Hazard. Mater.*, 250-251(2013), p. 238.
- [9] K. Yan, L.P. Liu, H.X. Zhao, L. Tian, Z.F. Xu, and R.X. Wang, Study on extraction separation of thioarsenite acid in alkaline solution by CO<sub>3</sub><sup>2-</sup>-type tri-n-octylmethyl-ammonium chloride, *Front. Chem.*, 8(2021), art. No. 592837.
- [10] K.Q. Li, J. Chen, J.H. Peng, M. Omran, and G. Chen, Efficient improvement for dissociation behavior and thermal decomposition of manganese ore by microwave calcination, *J. Clean. Prod.*, 260(2020), art. No. 121074.
- [11] X.L. Xi, M. Feng, L.W. Zhang, and Z.R. Nie, Applications of molten salt and progress of molten salt electrolysis in secondary metal resource recovery, *Int. J. Miner. Metall. Mater.*, 27(2020), No. 12, p. 1599.
- [12] H.F. Zhao, H.Y. Yang, L.L. Tong, Q. Zhang, and Y. Kong, Biooxidation-thiosulfate leaching of refractory gold concentrate, *Int. J. Miner. Metall. Mater.*, 27(2020), No. 8, p. 1075.
- [13] S.H. Yin, L.M. Wang, A.X. Wu, X. Chen, and R.F. Yan, Research progress in enhanced bioleaching of copper sulfides un-

- der the intervention of microbial communities, *Int. J. Miner. Metall. Mater.*, 26(2019), No. 11, p. 1337.
- [14] Z.Y. Ma, Y. Liu, J.K. Zhou, M.D. Liu, and Z.Z. Liu, Recovery of vanadium and molybdenum from spent petrochemical catalyst by microwave-assisted leaching, *Int. J. Miner. Metall. Mater.*, 26(2019), No. 1, p. 33.
- [15] H.H. Yi, Z.Y. Yang, X.L. Tang, S.Z. Zhao, F.Y. Gao, J.G. Wang, Y.H. Huang, K. Yang, Y.R. Shi, and X.Z. Xie, Variations of apparent activation energy based on thermodynamics analysis of zeolitic imidazolate frameworks including pyrolysis and combustion, *Energy*, 151(2018), p. 782.
- [16] H.D. Wang, S.H. Zhang, B. Li, D.A. Pan, Y.F. Wu, and T.Y. Zuo, Recovery of waste printed circuit boards through pyrometallurgical processing: A review, *Resour. Conserv. Recycl.*, 126(2017), p. 209.
- [17] B. Ebin and M.I. Isik, Pyrometallurgical processes for the recovery of metals from WEEE, [in] A. Chagnes, C. Ekberg, T. Retegan, G. Cote, and M. Nilsson, eds., *WEEE Recycling*, Elsevier, 2016, p.107.
- [18] C. Hagelūken, Recycling of electronic scrap at umicore's integrated metals smelter and refinery, *World Metall. ERZMETALL*, 59(2006), No. 3, p. 152.
- [19] K.Q. Li, Q. Jiang, L. Gao, J. Chen, J.H. Peng, S. Koppala, M. Omran, and G. Chen, Investigations on the microwave absorption properties and thermal behavior of vanadium slag: Improvement in microwave oxidation roasting for recycling vanadium and chromium, *J. Hazard. Mater.*, 395(2020), art. No. 122698.
- [20] Q.M. Wang, S.S. Wang, M. Tian, D.X. Tang, Q.H. Tian, and X.Y. Guo, Relationship between copper content of slag and matte in the SKS copper smelting process, *Int. J. Miner. Metall. Mater.*, 26(2019), No. 3, p. 301.
- [21] C. Quan, A.M. Li, and N.B. Gao, Research on pyrolysis of PCB waste with TG-FTIR and Py-GC/MS, *J. Therm. Anal. Calorim.*, 110(2012), No. 3, p. 1463.
- [22] C.C. Nie, Y.Y. Wang, H. Zhang, Y.K. Zhang, Y.Q. Zhang, Z.Q. Yan, B. Li, X.J. Lyu, Y.J. Tao, J. Qiu, L. Li, G.W. Zhang, and X.N. Zhu, Cleaner utilization of non-metallic components in separation tailings of waste printed circuit board: Pyrolysis oil, calorific value and building aggregate, *J. Clean. Prod.*, 258(2020), art. No. 120976.
- [23] R.T. Gao and Z.M. Xu, Pyrolysis and utilization of nonmetal materials in waste printed circuit boards: Debromination pyrolysis, temperature-controlled condensation, and synthesis of oil-based resin, *J. Hazard. Mater.*, 364(2019), p. 1.
- [24] K.Q. Li, G. Chen, X.T. Li, J.H. Peng, R. Ruan, M. Omran, and J. Chen, High-temperature dielectric properties and pyrolysis reduction characteristics of different biomass-pyrolusite mixtures in microwave field, *Bioresour. Technol.*, 294(2019), art. No. 122217.
- [25] R.R. Rajagopal, R. Rajarao, and V. Sahajwalla, High temperature transformations of waste printed circuit boards from computer monitor and CPU: Characterisation of residues and kinetic studies, *Waste Manage.*, 57(2016), p. 91.
- [26] R.T. Gao, Y. Liu, and Z.M. Xu, Synthesis of oil-based resin using pyrolysis oil produced by debromination pyrolysis of waste printed circuit boards, *J. Clean. Prod.*, 203(2018), p. 645.
- [27] X.W. Li, Q.Q. Mei, X.H. Dai, and G.J. Ding, Effect of anaerobic digestion on sequential pyrolysis kinetics of organic solid wastes using thermogravimetric analysis and distributed activation energy model, *Bioresour. Technol.*, 227(2017), p. 297.
- [28] R.R. Xiao, W. Yang, X.S. Cong, K. Dong, J. Xu, D.F. Wang, and X. Yang, Thermogravimetric analysis and reaction kinetics of lignocellulosic biomass pyrolysis, *Energy*, 201(2020), art. No. 117537.
- [29] F. Rego, A.P. Soares Dias, M. Casquilho, F.C. Rosa, and A. Rodrigues, Pyrolysis kinetics of short rotation coppice poplar biomass, *Energy*, 207(2020), art. No. 118191.
- [30] H. Fei, J.M. Shi, Y.L. Li, and Y. Liu, Precipitation characteristics of alkali metal of aquatic biomass in Poyang Lake during pyrolysis, *Nonferrous Met. Sci. Eng.*, 8(2017), No. 1, p. 139.
- [31] C. Zou, L.Y. Wen, J.X. Zhao, and R.M. Shi, Interaction mechanism between coal combustion products and coke in raceway of blast furnaces, *J. Iron Steel Res. Int.*, 24(2017), No. 1, p. 8.
- [32] H.L. Chiang and K.H. Lin, Exhaust constituent emission factors of printed circuit board pyrolysis processes and its exhaust control, *J. Hazard. Mater.*, 264(2014), p. 545.
- [33] J.E. White, W.J. Catallo, and B.L. Legendre, Biomass pyrolysis kinetics: A comparative critical review with relevant agricultural residue case studies, *J. Anal. Appl. Pyrol.*, 91(2011), No. 1, p. 1.
- [34] S. Sobek and S. Werle, Kinetic modelling of waste wood devolatilization during pyrolysis based on thermogravimetric data and solar pyrolysis reactor performance, *Fuel*, 261(2020), art. No. 116459.
- [35] A. Gupta, S.K. Thengane, and S. Mahajani, Kinetics of pyrolysis and gasification of cotton stalk in the central parts of India, *Fuel*, 263(2020), art. No. 116752.
- [36] K.Q. Li, Q. Jiang, G. Chen, L. Gao, J.H. Peng, Q. Chen, S. Koppala, M. Omran, and J. Chen, Kinetics characteristics and microwave reduction behavior of walnut shell-pyrolusite blends, *Bioresour. Technol.*, 319(2021), p. 124172.
- [37] J.J. Baeza-Baeza, C. Ortiz-Bolsico, and M.C. García-Álvarez-Coque, New approaches based on modified Gaussian models for the prediction of chromatographic peaks, *Anal. Chim. Acta*, 758(2013), p. 36.
- [38] S. Bernard, K. Fiaty, D. Cornu, P. Miele, and P. Laurent, Kinetic modeling of the polymer-derived ceramics route: Investigation of the thermal decomposition kinetics of poly[B-(methylamino)borazine] precursors into boron nitride, *J. Phys. Chem. B*, 110(2006), No. 18, p. 9048.
- [39] T.J. Chen, L.Y. Li, R.D. Zhao, and J.H. Wu, Pyrolysis kinetic analysis of the three pseudocomponents of biomass-cellulose, hemicellulose and lignin, *J. Therm. Anal. Calorim.*, 128(2017), No. 3, p. 1825.
- [40] X.J. Wang, J.Q. Wu, Y.M. Li, C.J. Zhou, and C.H. Xu, Pyrolysis kinetics and pathway of polysiloxane conversion to an amorphous SiOC ceramic, *J. Therm. Anal. Calorim.*, 115(2014), No. 1, p. 55.
- [41] K. Ding, *Numerical Simulation of Pyrolysis Characteristics and Process of Combustible Solid Waste* [Dissertation], Southeast University, Nanjing, 2017, p. 64.
- [42] Y.F. Shen, X.M. Chen, X.L. Ge, and M.D. Chen, Thermochemical treatment of non-metallic residues from waste printed circuit board: Pyrolysis vs. combustion, *J. Clean. Prod.*, 176(2018), p. 1045.
- [43] Z.W. Ye, F. Yang, W.X. Lin, S.P. Li, and S.Y. Sun, Improvement of pyrolysis oil obtained from co-pyrolysis of WPCBs and compound additive during two stage pyrolysis, *J. Anal. Appl. Pyrolysis*, 135(2018), p. 415.
- [44] C.H. Zhao, X.P. Zhang, and L. Shi, Catalytic pyrolysis characteristics of scrap printed circuit boards by TG-FTIR, *Waste Manage.*, 61(2017), p. 354.
- [45] X. Chen, *Infrared Absorption Spectroscopy and Application*, Shanghai Jiaotong University Press, Beijing, 1993, p. 46.
- [46] K.H. Lin and H.L. Chiang, Liquid oil and residual characteristics of printed circuit board recycle by pyrolysis, *J. Hazard. Mater.*, 271(2014), p. 258.
- [47] B. Janković, N. Manić, D. Stojiljković, and V. Jovanović, TSA-MS characterization and kinetic study of the pyrolysis process of various types of biomass based on the Gaussian multi-peak fitting and peak-to-peak approaches, *Fuel*, 234(2018), p. 447.
- [48] L. Huang, Y.C. Chen, G. Liu, S.N. Li, Y. Liu, and X. Gao, Non-isothermal pyrolysis characteristics of giant reed (*Arundo donax* L.) using thermogravimetric analysis, *Energy*, 87(2015), p. 31.